Published in final edited form as:
Chem Phys Lipids. 2010 September ; 163(7): 703–711. doi:10.1016/j.chemphyslip.2010.06.002.

Effects of the Endosomal Lipid Bis(monoacylglycero)phosphate on the Thermotropic Properties of DPPC: A ^{2}H NMR and Spin Label EPR Study

Thomas E. Frederick[†,‡], **Philip C. Goff**[†,‡], **Chad E. Mair**[£], **R. Suzanne Farver**[§], **Joanna R. Long**[§], and **Gail E. Fanucci**[†,*]

[†]Department of Chemistry, P.O. Box 117200, University of Florida, Gainesville Fl. 32611-7200

[§]Department of Biochemistry and Molecular Biology and McKnight Brain Institute, Box 100245, Gainesville, FL 32610-024

Abstract

Bis(monoacylglycero)phosphate (BMP) is an endosomal lipid with a unique structure that is implicated in the formation of intraendosomal vesicular bodies. Here we have characterized the effects of dioleoyl BMP ($BMP_{18:1}$) at concentrations of 5, 10, 15 and 20 mol% on the thermotropic behavior of dipalmitoyl phosphatidylcholine (DPPC) vesicles, and compared them to those of equimolar concentrations of dioleoyl phosphatidylglycerol (DOPG), a structural isoform of $BMP_{18:1}$. Because BMP is found in the acidic environments of the late endosome and intralysosomal vesicles, samples were prepared at pH 4.2 to mimic the pH of the lysosome. Both ^{2}H NMR of perdeuterated DPPC and spin-labeled EPR with 16-Doxyl phosphatidylcholine were utilized in these investigations. NMR and EPR results show that $BMP_{18:1}$ induces a lowering in the main phase transition temperature of DPPC similar to that of DOPG. The EPR studies reveal that $BMP_{18:1}$ induced more disorder in the L_β phase when compared to equimolar concentrations of DOPG. Analysis from dePaked ^{2}H NMR spectra in the L_α phase reveal that $BMP_{18:1}$ induces less disorder than equal concentrations of DOPG. Additionally, the results demonstrate that BMP mixes with other phospholipids as a phospholipid and not as a detergent molecule as once speculated.

Keywords

Lipid bilayers; LBPA; BMP; ^{2}H NMR; DPPC; mixed bilayers; spin-labeled lipids

1. Introduction

The biophysical principles behind complex membrane morphologies seen in cells and their internal organelles are a topic of increased interest in structural biology [1, 2]. In model lipid bilayer membranes, the curvature of the bilayer and the spontaneous shape of the resultant vesicle are dictated by the physical properties of the individual leaflets of the bilayer [3, 4].

[*]Corresponding author. Tel.: +1 352 392 2345; fax + 1 352 392 0872, fanucci@chem.ufl.edu (G.E. Fanucci).
[‡]These two authors contributed equally to this manuscript.
[£]Chad E. Mair's present address is Department of Chemistry, University of North Carolina, Chapel Hill, NC 27599-32901

Many of the biologically relevant morphologies seen within cells require membrane-protein interactions or controlled variation in lipid composition that can provide additional forces needed to overcome the intrinsic elastic properties of the lipid bilayer [1, 5, 6]. Lipid-mediated deformations can arise from a bilayer leaflet area mismatch or from lipid composition asymmetry [2, 7, 8]. Asymmetries in leaflet composition may give rise to differences in local bilayer spontaneous curvature, which could provide the necessary deformation for the onset of specific cellular events such as membrane fusion or vesicle budding [2, 9–11].

One example of lipid-mediate vesicle morphology is the *in vitro* generation of internal vesicular bodies when liposomes containing bis(monoacylglycero)phosphate (BMP) are subjected to a transmembrane pH gradient [12]. BMP, also known as lysobisphosphatidic acid (LBPA), is a unique anionic phospholipid whose chemical structure is shown in Figure 1. Although the concentration of BMP is less than 1% of the total lipid mass in cells, it comprises nearly 15% of the lipid composition of the acidic late endosome, which is currently the only known location of this lipid and where it is believed to be synthesized [13–15]. The unique *sn*-1-glycerophosphate-*sn*-1'-glycerol (*sn*1:*sn*1') stereoconfiguration found in BMP [16–20], as compared to the standard *sn*-3 stereoconfiguration of other phospholipids [21–23], limits the degradation of BMP by most phospholipases [16] and is thought to play a role in regulating the accumulation of BMP within the inner leaflet of the endosome limiting membrane [24]. Both the asymmetric distribution of BMP in the inner endosomal membrane and the pH gradient across the limiting membrane of late endosome have been implicated in the formation of the intraendosomal vesicular bodies seen *in vivo* [24].

BMP has increasingly been investigated for its role in late endosome structure and function [11, 13, 25–32]. Studies utilizing immuno-gold particles that label the anti-BMP monoclonal antibody demonstrate BMP localization within the intraendosomal vesicular body membranes [13]. Those results also show that anti-BMP antibodies disrupt the recycling process of the multifunctional receptor for mannose-6-phosphate-bearing ligands and insulin-like growth factor 2 (IGF2/MPR) between late endosomes and the *trans*-Golgi network resulting in their accumulation in the lab endosome, co-localized with BMP [13]. Furthermore, these antibodies induce the accumulation of cholesterol within the late endosome similar to that seen in Niemann-Pick syndrome [25, 26]. Combined, the IGF2/MPR and cholesterol results suggest that BMP plays a major role in late endosome sorting and trafficking functions. BMP is also important in regulating glycosphingolipid and ceramide degradation in the lysosome [27–29].

Considering the possible roles of BMP in endosome structure and function, as well as in glycosphingolipid and ceramide degradation, we are interested in knowing how BMP affects the thermotropic phase behavior and structural organization of model phosphatidylcholine (PC) lipid bilayer vesicles. Here we determine the effects that dioleoyl-BMP ($BMP_{18:1}$) has on the structural and thermotropic properties of dipalmitoyl phosphatidylcholine (DPPC) bilayers. We also compare its effects to dioleoyl phosphatidylglycerol (DOPG), an *sn*-3 structural isoform of $BMP_{18:1}$. Electron paramagnetic resonance (EPR) studies of DPPC/$BMP_{18:1}$ and DPPC/DOPG model membranes containing 16-doxyl-labeled PC provide a means to monitor the effects of either $BMP_{18:1}$ or DOPG on both the structural organization and the thermotropic phase behavior of DPPC. Specifically, we find from analysis of the EPR line shapes of the 16-doxyl label that $BMP_{18:1}$ induces more disorder than an equal molar concentration of DOPG to the methylene groups in the gel (L_β) phase. Solid-state ^2H nuclear magnetic resonance (NMR) investigations of samples containing acyl chain perdeuterated DPPC are complementary to the EPR investigations. Specifically, dePaking of ^2H NMR line shapes provides order parameters for each carbon position along the acyl

chain in the liquid crystalline (L_α) phase. The effects of $BMP_{18:1}$ on acyl chain ordering and dynamics in the melted phase of DPPC are similar to those of DOPG. From both the EPR and NMR data the effects of $BMP_{18:1}$ on the melting temperature of DPPC is found to be similar to that of DOPG.

2. Materials and Methods

2.1 Materials

DPPC (1,2-Dipalmitoyl-*sn*-Glycero-3-Phosphocholine), DPPC-d_{62} (1,2-Dipalmitoyl-d62-*sn*-Glycero-3-Phosphocholine), $BMP_{18:1}$ ((S,R Isomer) *sn*-(3-Oleoyl-2-Hydroxy)-Glycerol-1-Phospho-*sn*-3'-(1'-Oleoyl-2'-Hydroxy)-Glycerol, Ammonium Salt), 16-doxyl PC (1-Palmitoyl-2-Stearoyl-(16-DOXYL)-*sn*-Glycero-3-Phosphocholine), POPC (1-palmitoyl-2-oleoyl-*sn*-glycero-3-phosphocholine), and DOPG (1,2-dioleoyl-*sn*-glycero-3-phosphoglycerol) were purchased from Avanti Polar Lipids (Alabaster AL, USA) as chloroform solutions; all lipids were used without further purification. Phospholipid concentrations were verified utilizing a Malachite Green phosphate assay purchased from BioAssay Systems (Hawthorne, CA). NaOAc (sodium acetate, CH_3COONa), EDTA (ethylenediamine tetraacetic acid, $C_{10}H_{16}N_2O_8$), and NaCl (sodium chloride) were purchased from Fisher Biotech (Pittsburg, PA). CH_3Cl (chloroform), MeOH (methanol), clyclohexane, NH_4OH (ammonium hydroxide), HCl (hydrochloric acid), and NaOH (sodium hydroxide) were purchased from Fisher Scientific (Pittsburg, PA). Deuterium depleted water was purchased from Cambridge Isotope Laboratories Inc. (Andover MA, USA). Whatman TLC plates were silica coated aluminum and were purchased from Fisher (Pittsburg, PA). Structures of lipids utilized are shown in Figure 1.

2.2 Preparation of Phospholipid Vesicles

For all EPR and NMR sample preparations, the desired phospholipid mixtures were prepared in chloroform and dried either under a gentle nitrogen stream or rotary evaporation. Residual chloroform was removed by vacuum for four to six hours. The resulting lipid film was re-dissolved in a 4:1 cyclohexane:methanol mixture, subsequently flash frozen with liquid nitrogen, and lyophilized overnight. Lipids were hydrated in NaOAc buffer (pH 4.2) containing 50 mM NaOAc, 100 mM NaCl, 0.1 mM EDTA. Samples for EPR contained 1 mol% 16-doxyl PC with a total lipid concentration of 50 mM. Samples for ^{2}H NMR contained 25 mg total lipid (including 10 mg DPPC-d_{62}) and were suspended in 300 μL of deuterium depleted NaOAc buffer, pH 4.2, giving typical concentrations of 70 mM. During hydration, the lipid suspensions were incubated for one hour at 50 °C. Samples were subsequently passed through five freeze thaw cycles and vortex mixed at room temperature. Samples were stored at −20 °C. All samples were investigated as multilamellar vesicle (MLV) dispersions.

2.3 ^{2}H NMR Spectroscopy and ^{31}P NMR Spectroscopy

^{2}H NMR experiments were performed on a 500 MHz Bruker DRX spectrometer using a standard BBO probe. A quadrupole echo sequence (90°-τ-90°-τ-acq with τ = 30 μs) was used with a 40 kHz B_1 field (6.25 μs π/2 pulses). Typically 1024 transients, with a 0.5 s recycle delay, were collected. Spectra were collected over a range of ~10–50 °C in 2 °C increments for both $BMP_{18:1}$:DPPC and DOPG:DPPC mixtures, unless otherwise noted. The sample chamber temperature in the probe was calibrated using methanol and ethylene glycol standards. Samples were loaded in standard 5 mm NMR tubes. Wide line ^{31}P NMR spectra were collected using a two pulse Hahn echo sequence with typical pulse spacing of 40 μs, 4 μs π/2 pulses, with 25 kHz ^{1}H decoupling. A minimum of 1024 transients (5 μs dwell and 5 s recycle delay) were averaged for each spectrum. Spectra for POPC samples were performed with a Tecmag Apollo spectrometer operating at a resonance frequency of

145.2 MHz with a CP/MAS probe purchased from Doty Scientific, Inc., with variable temperature capability (± 1 °C). ^{31}P NMR spectra of DPPC samples were collected on a 500 MHz Bruker DRX system (Billerica, MA) using a standard 5 mm BBO probe. Phospholipid integrity both before and after NMR analysis was verified by thin layer chromatography (TLC) utilizing a 65:25:4 CH_3Cl:MeOH:NH_4OH mobile phase and development in an iodine chamber.

2.4 Electron Paramagnetic Resonance Spectroscopy

EPR spectroscopy was performed on a modified Bruker ER200 spectrometer with an ER023M signal channel, an ER 032M field control unit, and a loop gap resonator (Medical Advances, Milwaukee, WI). A quartz Dewar (Wilmad-Labglass) surrounded the loop gap resonator for variable temperature experiments; temperature was controlled by passing nitrogen gas through a copper coil submerged in a recirculating bath (Thermo Scientific) containing 40% ethylene glycol. Typically a sample volume of 10 μL was loaded into a 0.60 I.D. × 0.84 O.D. capillary tube.

2.5 Data Analysis

Moment analyses of the EPR and NMR data were utilized to determine the phase transition temperatures for all DPPC samples studied here. EPR spectra were phase corrected and normalized to the area under the absorption curve. The second moment (M_2) for each EPR spectrum was calculated and plotted as a function of temperature [33], while the first moment (M_1) of each ^{2}H NMR spectrum, was calculated and plotted as a function of temperature.

EPR and NMR moment plots were fit with either a Boltzmann sigmoid or a Double Boltzmann sigmoid function. The general form of a Boltzmann sigmoid function is:

$$y=\frac{A_1 - A_2}{1+e^{\frac{x-x_0}{dx}}}+A_2 \quad (1)$$

where A_1 and A_2 are the initial and final moment values respectively, x_0 corresponds to the temperature of the phase transition midpoint (defined as T_m), and dx defines the breadth of the Boltzmann sigmoid, which can be related to the $\Delta T_{1/2}$ of the phase transition by the equation:

$$\Delta T_{1/2}=dx \cdot \ln\left[\frac{3+2\sqrt{2}}{3-2\sqrt{2}}\right], \quad (2)$$

which is equivalent to the full width at half max of the derivative of Equation 1.

A sample whose moments as a function of temperature can be fit by a Boltzmann sigmoid is said to undergo a single first order transition; that is, the sample can be characterized by two states. If a Boltzmann sigmoid was insufficient to fit the moment plot, a Double Boltzmann sigmoid of the form:

$$y=y_0+A\left[\frac{f}{1+e^{\frac{x-x_1}{k_1}}}+\frac{1-f}{1+e^{\frac{x-x_2}{k_2}}}\right] \quad (3)$$

was used; this is interpreted as a system containing two phase transitions or three states. Here, y_0 is the lower limit of the fit equation, A is the difference between the global initial and final moments, f determines the relative magnitude of the two transitions, x_1 and x_2 are the midpoint of the first and second transition respectively, and k_1 and k_2 determine the

breadth of each transition. Similar to a single Boltzmann sigmoid, x_2 is defined as the second phase transition temperature, T_m, and k_2 is related to the breadth of the second phase transition, $\Delta T_{1/2}$, by Equation 2. Thermogram traces, which are analogous to differential scanning calorimetry plots, were generated using the first derivative of the fits.

NMR spectra were dePaked with previously published algorithms that utilize Tikhonov regularization to simultaneously determine dePaked spectra and magnetic alignment within the lipid vesicles [34]. When MLVs are subjected to a magnetic field, their alignment is assumed to be ellipsoidal [35, 36]. This assumption leads to the probability distribution function [34]:

$$p_{(E)}(\theta)\ \sin(\theta)[\,1-(1-\kappa_E)\cos^2\theta]^{-2} \quad (4)$$

where κ_E is the square of the ellipsoid's long to short axis ratio. Using an inverse transform to "dePake" spectra removes this orientation dependence and simplifies spectra of perdeuterated fatty acids. Furthermore, dePaked ^{2}H NMR spectra can then be used to determine the quadrupole splitting ($\Delta\upsilon_Q$) of the deuterium resonances, which can be assigned to individual C-D positions in DPPC [37]. A time-averaged order parameter $<S_{CD}>$ is then calculated from equation 5 [38].

$$\Delta\upsilon_Q=\frac{3}{4}\frac{e^2qQ}{h}(3\cos^2\theta-1)S_{CD} \quad (5)$$

The deuterium nucleus' quadrupole coupling to the electric field gradient, $\frac{3}{4}\frac{e^2qQ}{h}$, is assumed to be 167 kHz for each deuterated alkyl position [39]. The angle of the bilayer normal with respect to the magnetic field (θ) is zero as a result of the dePaking process.

3. Results

3.1 EPR Studies of 16-Doxyl PC in DPPC/BMP$_{18:1}$ and DPPC/DOPG Mixtures

EPR spectra were recorded over temperatures ranging from 10 to 50 °C in 0.5–2 °C increments for DPPC/BMP$_{18:1}$ samples containing 16-doxyl PC. Because BMP is found in the acidic environments of the late endosome and intralysosomal vesicles, samples were prepared at pH 4.2 which mimics the pH of the lysosome. For comparison, data were also collected for equal molar ratios of DPPC/DOPG mixtures. The chemical structure of BMP, DOPG, DPPC and the spin labeled lipid, 16-doxyl PC, are shown in Figure 1. The location of the spin label deep within the hydrocarbon interior of the bilayer is a useful probe of the L_β to L_α phase transition of DPPC [40, 41]. Characteristic spectra for 16-doxyl PC in the L_α and L_β phases of DPPC are shown in Figure 2. In the ordered L_β (gel) phase EPR spectra of 16-doxyl PC in DPPC are broad and anisotropic, particularly the high field transition, reflecting the presence of fewer gauche-trans isomerizations and slow axial diffusion. Significantly narrower and more isotropic line shapes are characteristic of the disordered L_α phase, where spin label motion is much less restricted. For pure DPPC, EPR spectra at 40 °C and 50 °C are indicative of the L_α phase, and for T < 40 °C, the spectra reflect slowing of motion and ordering, indicative of the formation of the L_β phase.

As expected, the addition of either BMP$_{18:1}$ or DOPG to DPPC is found to decrease the main phase transition temperature and lower the cooperativity of the phase transition (Fig 2 and 3). As shown in Figure 2, as the mol% of BMP$_{18:1}$ or DOPG is increased, the spectra for T < 40 °C are narrowed compared to pure DPPC, reflecting an increase in the disorder and mobility of the nitroxide spin label in these mixtures. These differences can be more readily

seen in plots of the spectral second moments (Fig. 3), which is a line shape parameter whose value scales as a function of the distance from the center of mass squared and the intensity; therefore, a higher second moment value indicates a slower correlation time that can be attributed to a more motionally restricted environment. For equimolar DPPC/$BMP_{18:1}$ and DPPC/DOPG samples, differences can be discerned in their EPR spectral line shapes, with the spectra for DPPC/$BMP_{18:1}$ broadened compared to the DPPC/DOPG samples, particularly for T < 40 °C. This effect is more clearly revealed in Figs 3C and 3D. This finding indicates that $BMP_{18:1}$ induces more disorder in the L_β phase than does an equal concentration of DOPG.

The second moment curves are readily fit by either single or double Boltzmann functions (Eq 1 and 2), and values of T_m and $\Delta T_{1/2}$ determined from these fits are given in Table 1. For DPPC containing 16-doxyl PC, T_m was determined from a fit over the limited temperature range of 33 °C to 50 °C and was found to be 39.5 ± 0.1 °C with a $\Delta T_{1/2}$ of 0.8 ± 0.3 °C. This value is slightly lower than the literature T_m value for DPPC (41.4 °C) obtained from both high sensitivity differential scanning calorimetry and dilatometry [42–45]; likely resulting from the slightly perturbing nature of the 1 mol% 16-doxyl PC nitroxide spin probe added to the system. The insets in Figure 3 show the corresponding thermogram curves that are plots of the derivative of the Boltzmann fits to the second moment data.

For pure DPPC samples and those containing 5 mol% $BMP_{18:1}$ or DOPG, the moment analysis data show inflections that correspond to the pretransition between the L_β and ripple (P_β) phases. For pure DPPC, the pretransition is detected at 30.1°C, which again differs slightly from the literature value of 35 °C [42, 44, 45], likely from the perturbing presence of the spin probe. For the 5 mol% $BMP_{18:1}$ and 5 mol% DOPG samples, the second moment plots are nicely fit over the entire temperature range with a double Boltzmann function (Equation 2) that provides temperatures for both the main phase transition and pretransition. The presence of the pretransition at this concentration indicates that both $BMP_{18:1}$ and DOPG are mixing with DPPC. As expected, when the concentration was increased to 15 mol% $BMP_{18:1}$ and 15 mol% DOPG samples, only a single Boltzmann population (i.e. two states) was needed for adequate fitting of the data.

Figures 3C and 3D compares the effects of $BMP_{18:1}$ to those of equimolar concentrations of DOPG. For all concentrations investigated, within error, both $BMP_{18:1}$ and DOPG decrease the main phase transition temperature of DPPC to the same extent. M_2 values converge to nearly the same point for $T > 40$ °C, but, for temperatures below the onset of the main phase transition ($T < 34$ °C) the M_2 values for spectra of samples containing $BMP_{18:1}$ are markedly lower than those containing the corresponding concentration of DOPG. Lower M_2 values correspond to an overall narrower EPR line shape that results from a greater degree of motional averaging of the spin label. Although equivalent concentrations of $BMP_{18:1}$ and DOPG appear to alter T_m as well as the breadth of the main phase transition to the same extent, $BMP_{18:1}$ is found to induce more disorder/mobility for the DPPC molecules in the L_β and P_β phases than does an equal molar concentration of DOPG.

3.2 ^{2}H NMR Comparison of BMP DPPC/$BMP_{18:1}$ and DPPC/DOPG Mixed Membranes

To further compare the effects of $BMP_{18:1}$ to DOPG on the organization and thermotropic phase behavior of DPPC model membranes, quadrupole echo ^{2}H NMR spectra were obtained every 2 °C over the temperature range of 10 °C to 50 °C for neat DPPC and DPPC/$BMP_{18:1}$ and DPPC/DOPG mixtures, where perdeuterated DPPC-d_{62} was used as the spectroscopic probe. As was done with the EPR samples, all samples were prepared at pH 4.2 to mimic the acidic environment of the lysosome. Figure 4A shows the ^{2}H NMR line shapes for neat DPPC at select temperatures. The ^{2}H NMR spectrum at 24 °C is characteristic of lipids in the lamellar gel phase, L_β; whereas the spectrum at 42 °C is

representative of lipids in the lamellar liquid, L_α, phase. Just as the 16-doxyl EPR experiments were able to discern the L_β to P_β phase transition, the ^2H NMR data also show evidence of this phase transition. Inspection of the ^2H NMR line shape at 34 °C (Figure 4A) reveals a resolved splitting of the terminal methyl peak region of the spectrum as compared to the non-split peaks seen at 24 °C. The onset of this spectral component occurs at 34 °C and is apparent until the main phase transition occurs at 39 °C. This agrees well with the L_β to P_β phase transition temperature of 35 °C determined by high sensitivity differential scanning calorimetry [42, 45]. The observed phase transition temperature of 39 °C is approximately 2 °C lower than the literature value for DPPC reported by differential scanning calorimetry; this effect is consistent with previous studies demonstrating that perdeuteration of the DPPC acyl chains will lower the P_β to L_α phase transition [46–49]. Note the spectrum of DPPC-d_{62} in DPPC at 39 °C reveals the coexistence of both the L_α and L_β phases (Figure 4), which have been described previously [50–53].

Figure 5 shows select ^2H NMR spectra over the temperature range of 24 °C to 42 °C of perdeuterated DPPC-d_{62} in DPPC liposome dispersions that contain increasing percentages of $BMP_{18:1}$ (top panel) or DOPG (bottom panel). Consistent with the EPR data, the ^2H NMR line shapes show that addition of either $BMP_{18:1}$ or DOPG both broadens the temperature range of the main phase transition and lowers T_m. Many of the ^2H NMR spectra in the L_α phase show enhanced perpendicular edge peaks and subdued perpendicular shoulder peaks. This effect arises from a macroscopic alignment of the liposome dispersions in the relatively high magnetic field of the spectrometer [35, 36]. It is noted, however, that for 15 mol% and 20 mol% BMP, there appears to be a lesser extent of macroscopic alignment of these samples. We have recently shown with dynamic light scattering (DLS) and transmission electron microscopy (TEM) that neat BMP forms small stable liposome structures [30] and induces small vesicle formation when mixed with gangliosides [54] and POPC [55]. We did not undertake DLS or TEM investigations here because of the difficulty in controlling the temperature in the DPPC system during DLS and TEM data acquisition. However, DLS and TEM images of POPC/BMP mixtures clearly show that incorporation of 15 mol% BMP induces the formation of liposome dispersions with smaller diameters (900 ± 200 nm) than those containing 20% POPG (1100 ± 300 nm) [55] or pure POPC (1400 ± 200 nm). The lesser alignment effects seen in the ^2H NMR spectra for the BMP containing samples is consistent with the interpretation that high concentrations of BMP lead to the formation of smaller liposome dispersions which would then have less of a tendency to orient within the magnetic field.

To obtain a more quantitative comparison of the effects of $BMP_{18:1}$ and DOPG on the phase transition temperatures, the first moment (M_1) of each ^2H NMR spectrum was calculated and plotted as a function of temperature. Upon addition of either $BMP_{18:1}$ (Figure 6A) or DOPG (Figure 6B), the main lipid phase transition decreases and broadens. M_1 plots were fit with a double Boltzmann sigmoid function (0%, 5% samples) or single Boltzmann function (10%, 15% and 20% samples). Figures 6C and 6D plot thermograms generated from the NMR data analysis, which were calculated from the derivative of the M_1 fits. Values for the main phase transition temperature, T_m, and the breadth of the transition, $\Delta T_{1/2}$, were also determined from the first moment data and are reported in Table 1. There is overall good agreement between the NMR and EPR results.

The effects of $BMP_{18:1}$ and DOPG on the acyl chain order of DPPC in the L_α phase were further characterized by calculating the order parameter $\langle S_{CD} \rangle$ for each carbon position at 44 °C by measuring the quadrupole splittings ($\Delta \upsilon_Q$) from Depaked NMR spectra. Because of the alignment of the vesicles with the magnetic field, a depaking algorithm that accounted for this affect was utilized [34]. Figures 6E and 6F plot values of $\langle S_{CD} \rangle$ for DPPC/$BMP_{18:1}$ and DPPC/DOPG mixtures; respectively. As the concentration of DOPG increases, the

$<S_{CD}>$ parameter value is shown to slightly decrease, indicative of increasing disorder in the acyl chains. However the DPPC order parameter values are relatively invariant as a function of increasing $BMP_{18:1}$ concentration, indicating that when melted $BMP_{18:1}$ packs similarly to DPPC or that in the L_α phase $BMP_{18:1}$ is excluded from DPPC enriched domains.

3.3 ^{31}P NMR spectra of $BMP_{18:1}$ and DOPG mixtures

In order to investigate whether $BMP_{18:1}$ is demixing with PC lipids, ^{31}P NMR spectra were obtained. Figure 7A shows wide-line ^{31}P NMR spectra for POPC/$BMP_{18:1}$ mixtures at 27 °C. The line shapes for 100% $BMP_{18:1}$ and 100% POPC are indicative of lamellar bilayer phases [56]. The narrowed span of the $BMP_{18:1}$ spectrum reflects an orientation of the phosphate group that is altered from that in POPC, and the NMR results are consistent with molecular dynamic simulations [30, 31]. For the mixtures, as the mol% of $BMP_{18:1}$ is increased, the overall span of the POPC spectrum narrows indicating that $BMP_{18:1}$ is mixing with POPC over this concentration range. Figure 7B shows how the span, $\Delta\sigma$, of the POPC spectrum narrows linearly as the mole fraction of $BMP_{18:1}$ is increased. This behavior is consistent with previous work of Seelig and Scherer, who showed that when charged lipids are mixed with PC bilayers that the electrostatic effects alter the angular orientation of the PC head group with respect to the bilayer normal [57]. The altered orientation results in a narrowing in the span of the ^{31}P line shape [58–60]. Hence, the narrowing of both the POPC and BMP spectra from their 100% line shapes indicates that the two lipids are interacting (i.e. mixed) with each other in the multilamellar liposome preparations and that when $BMP_{18:1}$ is mixed with POPC it has a similar effect on the average orientation of the head group with the bilayer normal as other negatively charged lipids [57, 61].

Figure 7C and 7D show ^{31}P NMR spectra of $BMP_{18:1}$ and DOPG mixed with DPPC at pH 4.2; respectively. Here, the spectra were collected at 47 °C, to ensure that samples were in the L_α phase. As can be seen, the DPPC spectrum narrows upon incorporation of either $BMP_{18:1}$ or DOPG, and that the narrowing is enhanced at higher concentration of negatively charged lipid incorporation. Note, the ^{31}P lineshape for BMP is a narrowed lamellar pattern (as shown in Fig 7A), and not an isotropic signal. These findings clearly show that $BMP_{18:1}$ is not demixing with DPPC in the L_α and that the ^{2}H NMR data in Figure 6E imply that $BMP_{18:1}$ packs similarly to DPPC in the L_α phase.

4. Discussion

4.1 BMP Mixes with DPPC and does not act like a detergent

These results clearly demonstrate that BMP does not have detergent like properties when mixed with PC lipids. Based upon the shape hypothesis of lipid polymorphisms [62], the unusual chemical connectivity of BMP was speculated to be either a “cone-like” geometry, that is having properties similar to phosphatidylethanolamines which increase lateral pressure profiles that can induce hexagonal phase mesostructures, or an “inverted-cone” geometry, predicting properties similar to detergent molecules that can form micelles or solubilize lipid bilayers [11]. Reported experimental investigations and molecular dynamic simulations of dimyristoyl BMP, ($BMP_{14:0}$), show that BMP adopts a lamellar bilayer organization when hydrated [31]. Recent work from our lab has also shown that hydrated $BMP_{18:1}$ adopts a lamellar bilayer mesophase and can be extruded into vesicles that can trap fluorescence molecules in the inner compartment; consistent with a large unilamellar vesicle structure [30]. Clearly, the combined EPR and NMR work presented here demonstrate that BMP mixes with DPPC to form a lamellar mesophase very similar in lipid packing as DOPG/DPPC mixtures. In addition, BMP mixtures with gangliosides have been shown to adopt a lamellar structures by freeze-fracture electron microscopy, small-angle x-ray scattering [32] and EPR investigations [54]. Taken together, these combined biophysical

studies show that although BMP has an unusual head group configuration and acyl-chain connectivity, it packs similarly to other phospholipids, such as its isoform DOPG, in hydrated bilayers and does not act like a detergent. Interestingly, however, BMP induces more disorder in the gel phase of DPPC than does DOPG, but doesn't appear to affect the acyl chain order in the melting liquid crystalline phase.

4.2 Comparison of NMR and EPR results and Tm values

In this study, both ^{2}H NMR and spin-labeled EPR were used to investigate local dynamics and acyl-chain packing. Both methods give relatively good agreement in reporting on the main phase transition temperature and the cooperativity of the phase transitions. When data are collected over small temperature increments with adequate thermal stabilizations, both methods clearly reveal the pretransition in the pure DPPC samples and lower mixtures. In addition, the 16-doxyl moiety doesn't appear to lower the main phase transition any more than the fully deuterated DPPC molecule. However, the 16-doxyl moiety appears to induce greater $\Delta T_{1/2}$ values compared to perdeuterated DPPC-d_{62}; this may result from the location of 16-doxyl spin-label within the bilayer. Given that the EPR and ^{2}H NMR time scales vary, it is not surprising that the two methods provide complimentary, but different, information about the lipid systems. In particular, the EPR data are shown to be more sensitive to slower motions that occur in the gel phase, whereas the ^{2}H NMR line shapes are more sensitive to faster motional fluctuations in the liquid-crystalline phase. To our knowledge, there are very few reports in the membrane biophysics literature or in lipid-peptide interactions where both ^{2}H NMR and spin-labeled lipids and EPR spectroscopy are used in a complimentary manner. Our results indicate that both methods, used together, can provide a more complete picture on how lipid packing and dynamics are altered as a function of either lipid composition or small molecule/peptide/protein interactions.

5. Conclusions

These EPR and ^{2}H NMR studies reveal that $BMP_{18:1}$ disrupts the L_β phase packing of DPPC to a further extent than DOPG, which is a structural isomer of $BMP_{18:1}$but minimally affects DPPC acyl chain dynamics in the L_α phase. Interestingly, the EPR and ^{2}H NMR measurements are sensitive to different aspects of the interaction of $BMP_{18:1}$ or DOPG with DPPC. For the EPR work reported here, the molecular probe used is a nitroxide spin label that has been engineered at the carbon 16 position along the acyl chain. On the other hand, fully deuterated DPPC was used as the spectroscopic probe for ^{2}H NMR investigations. Both methods provide similar values for the main phase transition melting temperature and breadths of the melting transitions, indicating that the EPR spin probe is no more perturbing than the fully deuterated acyl-chains. However, given that the time scale of the two measurements differs, we observe with EPR that $BMP_{18:1}$ disrupts the gel phase order to a greater extent than does DOPG.

Furthermore, ^{2}H NMR $\langle S_{CD} \rangle$ order parameters reveal that $BMP_{18:1}$ minimally affects the acyl chain dynamics of DPPC in the L_α phase; which may indicate some demixing of $BMP_{18:1}$ from DPPC, although the ^{31}P NMR line shapes in the liquid crystalline phase report on bulk mixing. Previous dynamic light scattering and negative staining transmission electron microscopy studies of neat $BMP_{18:1}$ membranes have shown that this unique phospholipid tends to form multilamellar and large unilamellar vesicles with a greater positive curvature than typical phosphatidylcholine and phosphatidylglycerol vesicles [30]. The ability of $BMP_{18:1}$ to demix from other phospholipids and its tendency to form more positively curved vesicles may provide the necessary forces for the *in vivo* generation of vesicular bodies in late endosomes.

Acknowledgments

The research herein was funded by NIH R01GM077232 (GEF) and R01HL076586 (JRL). We are grateful to E. Sternin for access to his ^{2}H NMR dePaking programs.

Abbreviations

LBPA	lysobisphosphatidic acid
BMP	bis(monoacylglycerol)phosphate
$BMP_{18:1}$	(S,R Isomer) *sn*-(3-Oleoyl-2-Hydroxy)-Glycerol-1-Phospho-*sn*-3'-(1'-Oleoyl-2'-Hydroxy)-Glycerol
DPPC	1,2-Dipalmitoyl-*sn*-Glycero-3-Phosphocholine
DPPC-d_{62}	1,2-Dipalmitoyl-D62-*sn*-Glycero-3-Phosphocholine
NMR	nuclear magnetic resonance
EPR	electron paramagnetic resonance
MLV	multilamellar vesicle

References

1. Zimmerberg J, Kozlov MM. How proteins produce cellular membrane curvature. Nat Rev Mol Cell Bio. 2006; 7:9–19. [PubMed: 16365634]
2. Farsad K, De Camilli P. Mechanisms of membrane deformation. Curr Opin Cell Biol. 2003; 15:372–381. [PubMed: 12892776]
3. Zimmerberg J. Are the curves in all the right places? Traffic. 2000; 1:366–368. [PubMed: 11208121]
4. Chernomordik LV, Kozlov MM. Protein-lipid interplay in fusion and fission of biological membranes. Annu Rev Biochem. 2003; 72:175–207. [PubMed: 14527322]
5. Hamm M, Kozlov MM. Elastic energy of tilt and bending of fluid membranes. Eur Phys J E. 2000; 3:323–335.
6. May S. Protein-induced bilayer deformations: the lipid tilt degree of freedom. Eur Biophys J Biophy. 2000; 29:17–28.
7. Sheetz MP, Singer SJ. Biological-Membranes as Bilayer Couples - Molecular Mechanism of Drug-Erythrocyte Interactions. P Natl Acad Sci USA. 1974; 71:4457–4461.
8. Devaux PF. Is lipid translocation involved during endo- and exocytosis? Biochimie. 2000; 82:497–509. [PubMed: 10865135]
9. Burger KNJ. Greasing membrane fusion and fission machineries. Traffic. 2000; 1:605–613. [PubMed: 11208148]
10. Farge E, Ojcius DM, Subtil A, Dautry-Varsat A. Enhancement of endocytosis due to aminophospholipid transport across the plasma membrane of living cells. Am J Physiol-Cell Ph. 1999; 276:C725–C733.
11. Holopainen JM, Angelova MI, Kinnunen PKJ. Vectorial budding of vesicles by asymmetrical enzymatic formation of ceramide in giant liposomes. Biophys J. 2000; 78:830–838. [PubMed: 10653795]
12. Matsuo H, Chevallier J, Mayran N, Le Blanc I, Ferguson C, Faure J, Blanc NS, Matile S, Dubochet J, Sadoul R, Parton RG, Vilbois F, Gruenberg J. Role of LBPA and Alix in multivesicular liposome formation and endosome organization. Science. 2004; 303:531–534. [PubMed: 14739459]
13. Kobayashi T, Stang E, Fang KS, de Moerloose P, Parton RG, Gruenberg J. A lipid associated with the antiphospholipid syndrome regulates endosome structure and function. Nature. 1998; 392:193–197. [PubMed: 9515966]

14. Kobayashi T, Startchev K, Whitney AJ, Gruenberg J. Localization of lysobisphosphatidic acid-rich membrane domains in late endosomes. Biol Chem. 2001; 382:483–485. [PubMed: 11347897]
15. Kobayashi T, Beuchat MH, Chevallier J, Makino A, Mayran N, Escola JM, Lebrand C, Cosson P, Kobayashi T, Gruenberg J. Separation and characterization of late endosomal membrane domains. J Biol Chem. 2002; 277:32157–32164. [PubMed: 12065580]
16. Brotheru J, Renkonen O. Novel Stereoconfiguration in Lyso-Bis-Phosphatidic Acid of Cultured Bhk-Cells. Chem Phys Lipids. 1974; 13:178–182. [PubMed: 4473276]
17. Joutti A, Brotherus J, Renkonen O, Laine R, Fischer W. Stereochemical Configuration of Lysobisphosphatidic Acid from Rat-Liver, Rabbit Lung and Pig Lung. Biochim Biophys Acta. 1976; 450:206–209. [PubMed: 990300]
18. Joutti A. Stereoconfiguration of Newly Formed Molecules of Bis(Monoacylglycero)Phosphate in Bhk Cells. Biochim Biophys Acta. 1979; 575:10–15. [PubMed: 508774]
19. Joutti A, Renkonen O. Stereo-Configuration of Bis(Monoacylglycero)Phosphate Synthesized Invitro in Lysosomes of Rat-Liver - Comparison with the Natural Lipid. J Lipid Res. 1979; 20:840–847. [PubMed: 490056]
20. Joutti A, Renkonen O. Stereochemical Configuration of Lysosomal Phosphatidylcholine and Phosphatidylethanolamine - Comparison with Lysobisphosphatidic Acid. J Lipid Res. 1979; 20:230–233. [PubMed: 438662]
21. Kolter T, Sandhoff K. Principles of lysosomal membrane digestion: Stimulation of sphingolipid degradation by sphingolipid activator proteins and anionic lysosomal lipids. Annu Rev Cell Dev Bi. 2005; 21:81–103.
22. Gennis, RB. Biomembranes Molecular Structure and Function. 1989.
23. Yeagle, PL. The Structure of Biological Membranes. 2005. ed.
24. Simons K, Gruenberg J. Jamming the endosomal system: lipid rafts and lysosomal storage diseases. Trends Cell Biol. 2000; 10:459–462. [PubMed: 11050411]
25. Kobayashi T, Beuchat MH, Lindsay M, Frias S, Palmiter RD, Sakuraba H, Parton RG, Gruenberg J. Late endosomal membranes rich in lysobisphosphatidic acid regulate cholesterol transport. Nat Cell Biol. 1999; 1:113–118. [PubMed: 10559883]
26. Delton-Vandenbroucke I, Bouvier J, Makino A, Besson N, Pageaux JF, Lagarde M, Kobayashi T. Anti-bis(monoacylglycero) phosphate antibody accumulates acetylated LDL-derived cholesterol in cultured macrophages. J Lipid Res. 2007; 48:543–552. [PubMed: 17146116]
27. Wilkening G, Linke T, Uhlhorn-Dierks G, Sandhoff K. Degradation of membrane-bound ganglioside GM1 - Stimulation by bis(monoacylglycero)phosphate and the activator proteins SAP-B and GM2-AP. J Biol Chem. 2000; 275:35814–35819. [PubMed: 10942779]
28. Werth N, Schuette CG, Wilkening G, Lemm T, Sandhoff K. Degradation of membrane-bound ganglioside GM2 by beta-hexosaminidase A - Stimulation by GM2 activator protein and lysosomal lipids. J Biol Chem. 2001; 276:12685–12690. [PubMed: 11278374]
29. Linke T, Wilkening G, Sadeghlar F, Mozcall H, Bernardo K, Schuchman E, Sandhoff K. Interfacial regulation of acid ceramidase activity - Stimulation of ceramide degradation by lysosomal lipids and sphingolipid activator proteins. J Biol Chem. 2001; 276:5760–5768. [PubMed: 11104761]
30. Frederick TE, Chebukati JN, Mair CE, Goff PC, Fanucci GE. Bis(monoacylglycero)phosphate Forms Stable Small Lamellar Vesicle Structures: Insights into Vesicular Body Formation in Endosomes. Biophys J. 2009; 96
31. Hayakawa T, Hirano Y, Makino A, Michaud S, Lagarde M, Pageaux JF, Doutheau A, Ito K, Fujisawa T, Takahashi H, Kobayashi T. Differential membrane packing of stereoisomers of bis(monoacylglycero)phosphate. Biochemistry. 2006; 45:9198–9209. [PubMed: 16866366]
32. Hayakawa T, Makino A, Murate M, Sugimoto I, Hashimoto Y, Takahashi H, Ito K, Fujisawa T, Matsuo H, Kobayashi T. pH-dependent formation of membranous cytoplasmic body-like structure of ganglioside G(M1)/bis(monoacylglycero)phosphate mixed membranes. Biophys J. 2007; 92:L13–L16. [PubMed: 17056735]
33. Slichter, CP. Principles of Magnetic Resonance. 2nd ed.. Berlin: Springer-Verlag; 1978.

34. Sternin E, Schafer H, Polozov IV, Gawrisch K. Simultaneous determination of orientational and order parameter distributions from NMR spectra of partially oriented model membranes. J Magn Reson. 2001; 149:110–113. [PubMed: 11273758]
35. Seelig J, Borle F, Cross TA. Magnetic-Ordering of Phospholipid-Membranes. Biochim Biophys Acta. 1985; 814:195–198.
36. Qiu XX, Mirau PA, Pidgeon C. Magnetically Induced Orientation of Phosphatidylcholine Membranes. Biochim Biophys Acta. 1993; 1147:59–72. [PubMed: 8466932]
37. Seelig A, Seelig J. Dynamic Structure of Fatty Acyl Chains in a Phospholipid Bilayer Measured by Deuterium Magnetic-Resonance. Biochemistry-Us. 1974; 13:4839–4845.
38. Seelig J, Seelig A. Lipid Conformation in Model Membranes and Biological-Membranes. Q Rev Biophys. 1980; 13:19–61. [PubMed: 7220788]
39. Burnett LJ, Muller BH. Deuteron Quadrupole Coupling Constants in 3 Solid Deuterated Paraffin Hydrocarbons-C2d6, C4d10, C6d14. J Chem Phys. 1971; 55:5829. &.
40. Riske KA, Fernandez RM, Nascimento OR, Bales BL, Lamy-Freund MT. DMPG gel-fluid thermal transition monitored by a phospholipid spin labeled at the acyl chain end. Chem Phys Lipids. 2003; 124:69–80. [PubMed: 12787945]
41. Vogel A, Scheidt HA, Huster D. The distribution of lipid attached spin probes in bilayers: application to membrane protein topology. Biophys J. 2003; 85:1691–1701. [PubMed: 12944284]
42. Tristram-Nagle S, Nagle JF. Lipid bilayers: thermodynamics, structure, fluctuations, and interactions. Chem Phys Lipids. 2004; 127:3–14. [PubMed: 14706737]
43. Nagle JF, Wilkinson DA. Lecithin Bilayers: Density Measurements and Molecular Interactions. Biophys J. 1978; 23:159–175. [PubMed: 687759]
44. Tristram-Nagle S, Wiener MC, Yang CP, Nagle JF. Kinetics of the Subtransition in Dipalmitoylphosphatidylcholine. Biochemistry-Us. 1987; 26:4288–4294.
45. Mabrey S, Sturtevant JM. Investigation of Phase-Transitions of Lipids and Lipid Mixtures by High Sensitivity Differential Scanning Calorimetry. P Natl Acad Sci USA. 1976; 73:3862–3866.
46. Petersen NO, Kroon PA, Kainoshio M, Chan SI. Thermal phase transitions in deuterated lecithin bilayers. Chem Phys Lipids. 1975; 14:343–349. [PubMed: 1175255]
47. Davis JH. Deuterium magnetic resonance study of the gel and liquid crystalline phases of dipalmitoyl phosphatidylcholine. Biophys J. 1979; 27:339–358. [PubMed: 263690]
48. Vist MR, Davis JH. Phase-Equilibria of Cholesterol Dipalmitoylphosphatidylcholine Mixtures – H-2 Nuclear Magnetic-Resonance and Differential Scanning Calorimetry. Biochemistry-Us. 1990; 29:451–464.
49. Scheidt HA, Huster D, Gawrisch K. Diffusion of cholesterol and its precursors in lipid membranes studied by H-1 pulsed field gradient magic angle spinning NMR. Biophys J. 2005; 89:2504–2512. [PubMed: 16085761]
50. Huschilt JC, Hodges RS, Davis JH. Phase-Equilibria in an Amphiphilic Peptide Phospholipid Model Membrane by Deuterium Nuclear Magnetic-Resonance Difference Spectroscopy. Biochemistry-Us. 1985; 24:1377–1386.
51. Linseisen FM, Thewalt JL, Bloom M, Bayerl TM. H-2-Nmr and Dsc Study of Sepc-Cholesterol Mixtures. Chem Phys Lipids. 1993; 65:141–149.
52. Hsueh YW, Gilbert K, Trandum C, Zuckermann M, Thewalt J. The effect of ergosterol on dipalmitoylphosphatidylcholine bilayers: A deuterium NMR and calorimetric study. Biophys J. 2005; 88:1799–1808. [PubMed: 15596499]
53. Thewalt JL, Bloom M. Phosphatidylcholine: cholesterol phase diagrams. Biophys J. 1992; 63:1176–1181. [PubMed: 19431848]
54. Chebukati JN, Goff PC, Frederick TE, Fanucci GE. Bis(monoacylglycero)phosphate and ganglioside GM1 spontaneously form small homogeneous vesicles at specific concentrations. Biochem Biophys Res Commun. 2010; 394:509–514. [PubMed: 20206128]
55. Chebukati, JN. Chemistry. Gainesville, FL: University of Florida; 2009.
56. Neiderberger W, Seelig J. Phosphorus-31 chemical shift anisotropy in unsonicated phospholipid bilayers. Journal of the American Chemical Society. 1976; 98:3704–3706. [PubMed: 946807]

57. Scherer PG, Seelig J. Electric Charge Effects on Phospholipid Headgroups - Phosphatidylcholine in Mixtures with Cationic and Anionic Amphiphiles. Biochemistry-Us. 1989; 28:7720–7728.

58. Gally HU, Niederberger W, Seelig J. Conformation and Motion of Choline Head Group in Bilayers of Dipalmitoyl-3-Sn-Phosphatidylcholine. Biochemistry-Us. 1975; 14:3647–3652.

59. Seelig J. P-31 Nuclear Magnetic-Resonance and Head Group Structure of Phospholipids in Membranes. Biochim Biophys Acta. 1978; 515:105–140. [PubMed: 356883]

60. Griffin RG, Powers L, Pershan PS. Head-Group Conformation in Phospholipids – P-31 Nuclear Magnetic-Resonance Study of Oriented Monodomain Dipalmitoylphosphatidylcholine Bilayers. Biochemistry-Us. 1978; 17:2718–2722.

61. Mair, CE. Chemistry. Gainesville, FL: University of Florida; 2008.

62. Gruner SM, Cullis PR, Hope MJ, Tilcock CP. Lipid polymorphism: the molecular basis of nonbilayer phases. Annu Rev Biophys Biophys Chem. 1985; 14:211–238. [PubMed: 3890880]

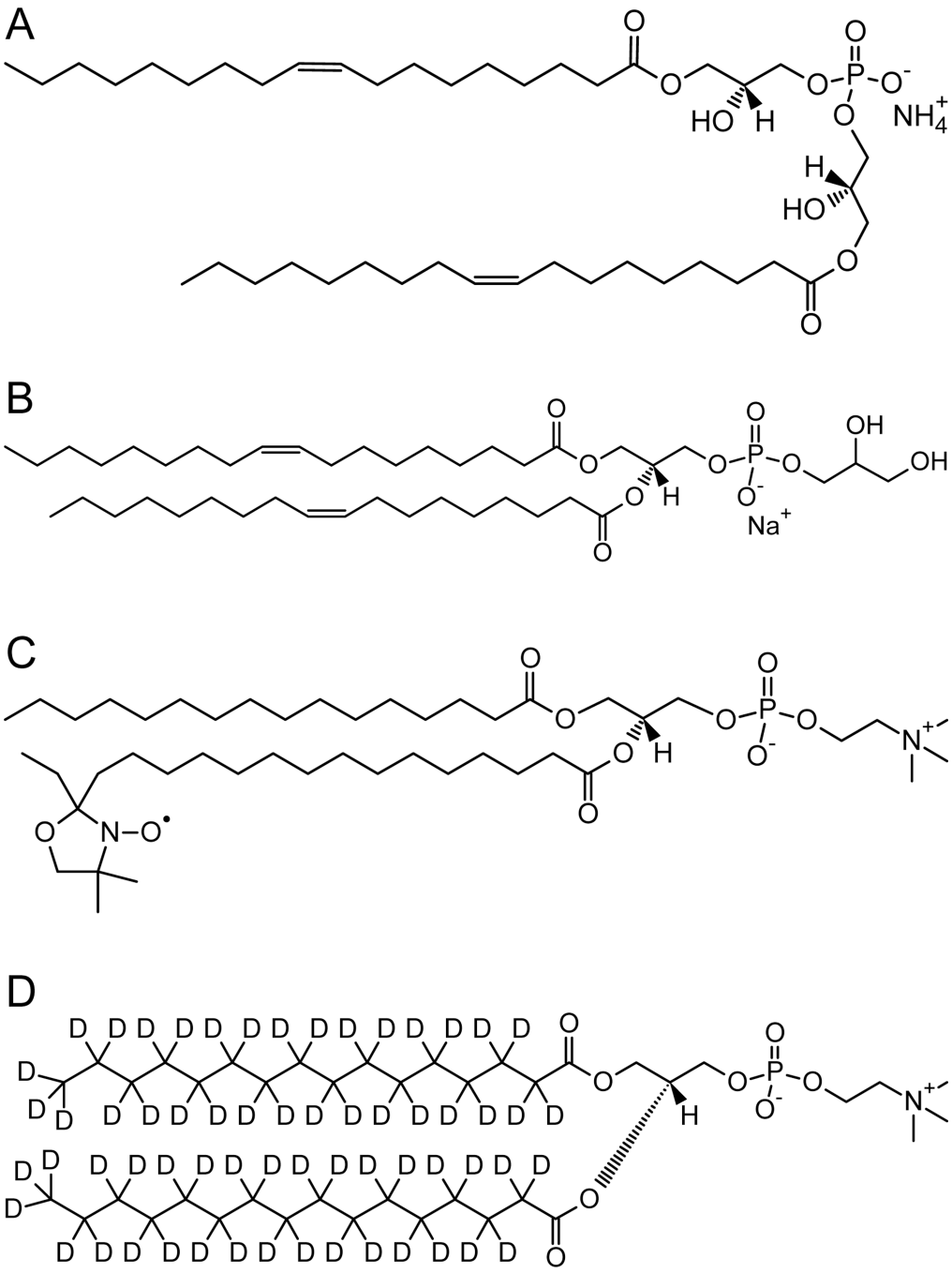

FIGURE 1.
Phospholipids employed in this study: (A) $BMP_{18:1}$, (B) DOPG, (C) 16-doxyl PC, and (D) DPPC-d_{62}.

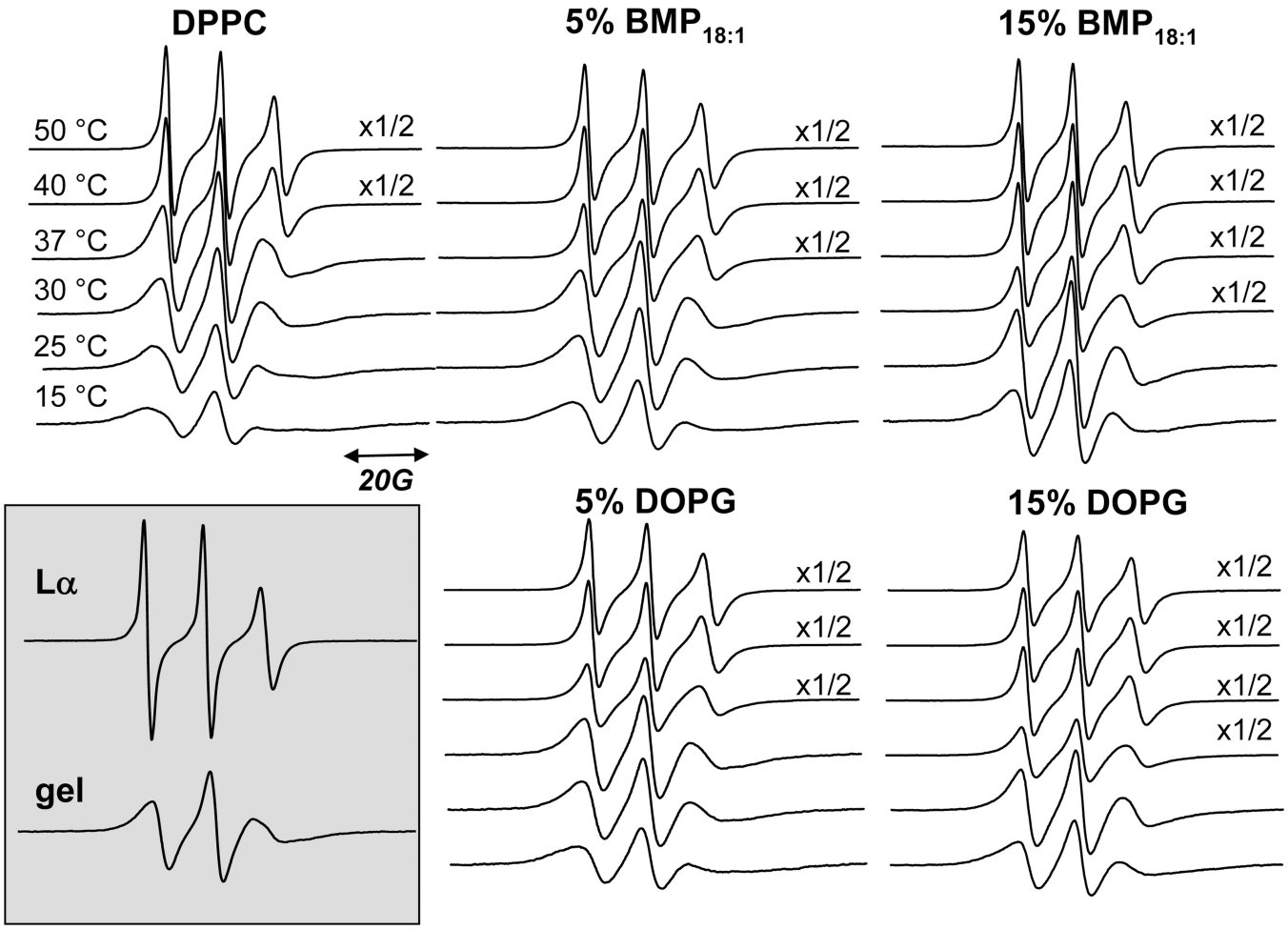

FIGURE 2.

X-band EPR spectra of 1 mol% 16-doxyl PC in DPPC in the L_β phase at 25 °C and the L_α phase at 50 °C. Stack plots showing select EPR spectral line shapes for 1 mol% 16-doxyl PC incorporated into DPPC mixtures containing either 5 mol% or 15 mol% $BMP_{18:1}$ or 5 mol% or 15 mol% DOPG as indicated. Spectra are intensity scaled to normalize the integral areas and were collected with 2 mW incident microwave power, 1.8 G modulation amplitude and a scan width of 100 G. Spectra were collected at the same temperatures as indicated for DPPC. For clarity of presentation, the intensity of select spectra were scaled by a factor of 1/2 as noted.

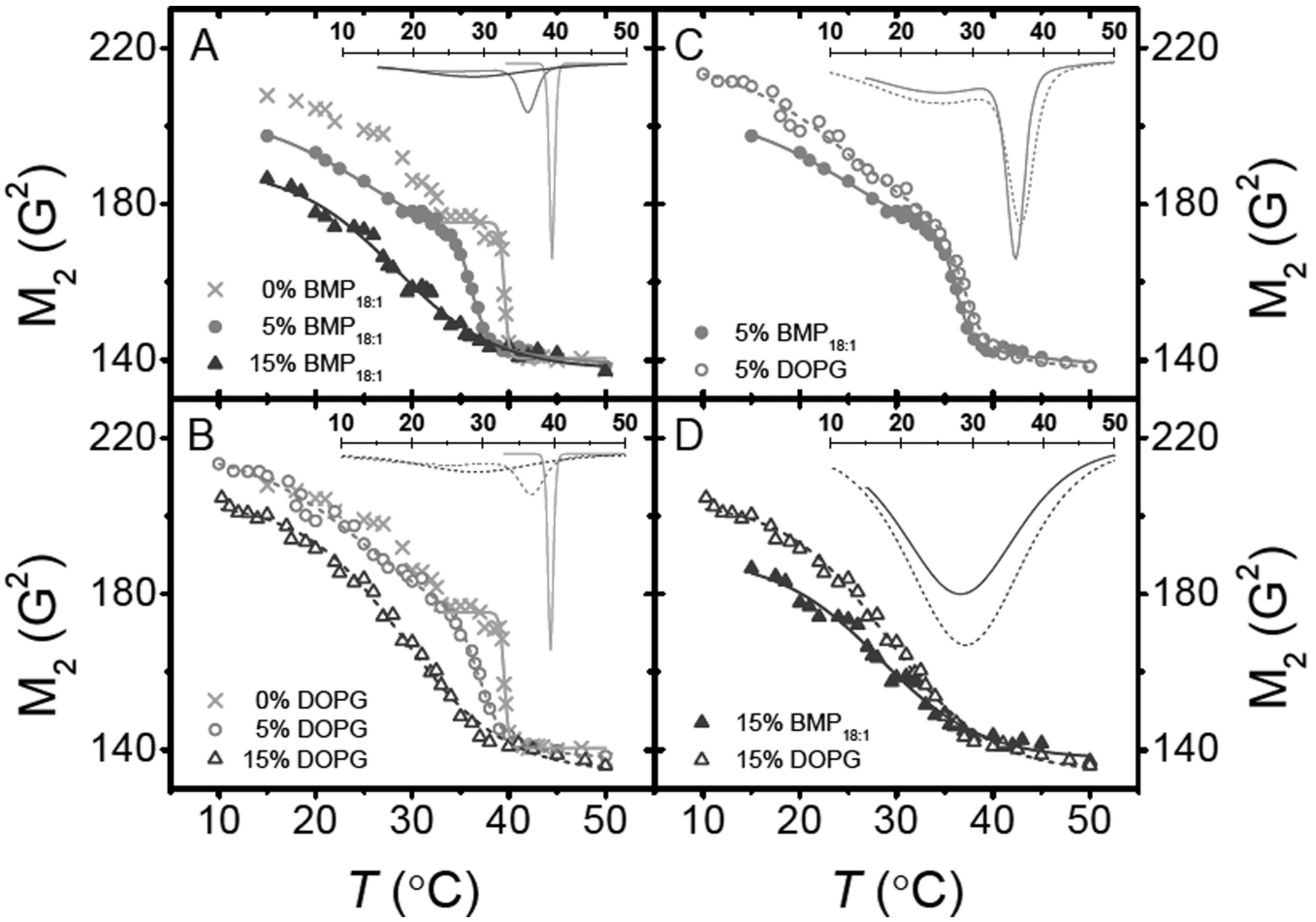

FIGURE 3.

Second moment, M_2, analysis of EPR spectral line shapes of 16-doxyl PC in (A) DPPC/$BMP_{18:1}$ and in (B) DPPC/DOPG mixtures. The second moment is defined as $\sum(x_n\text{-}x_o)^2 I_n$, where x_o is the center of mass of the spectrum and where I_n is the intensity at point x_n. In all figures solid lines through data points represent best fits to the data using either a single of double Boltzmann function as described within the text. Corresponding thermal melting curves are plotted near the top of each figure. (C) Comparison of effects of 5 mol% $BMP_{18:1}$ to 5 mol% DOPG in the melting behavior of DPPC. (D) Comparison of the effects of 15 mol % $BMP_{18:1}$ to 15 mol% DOPG in DPPC.

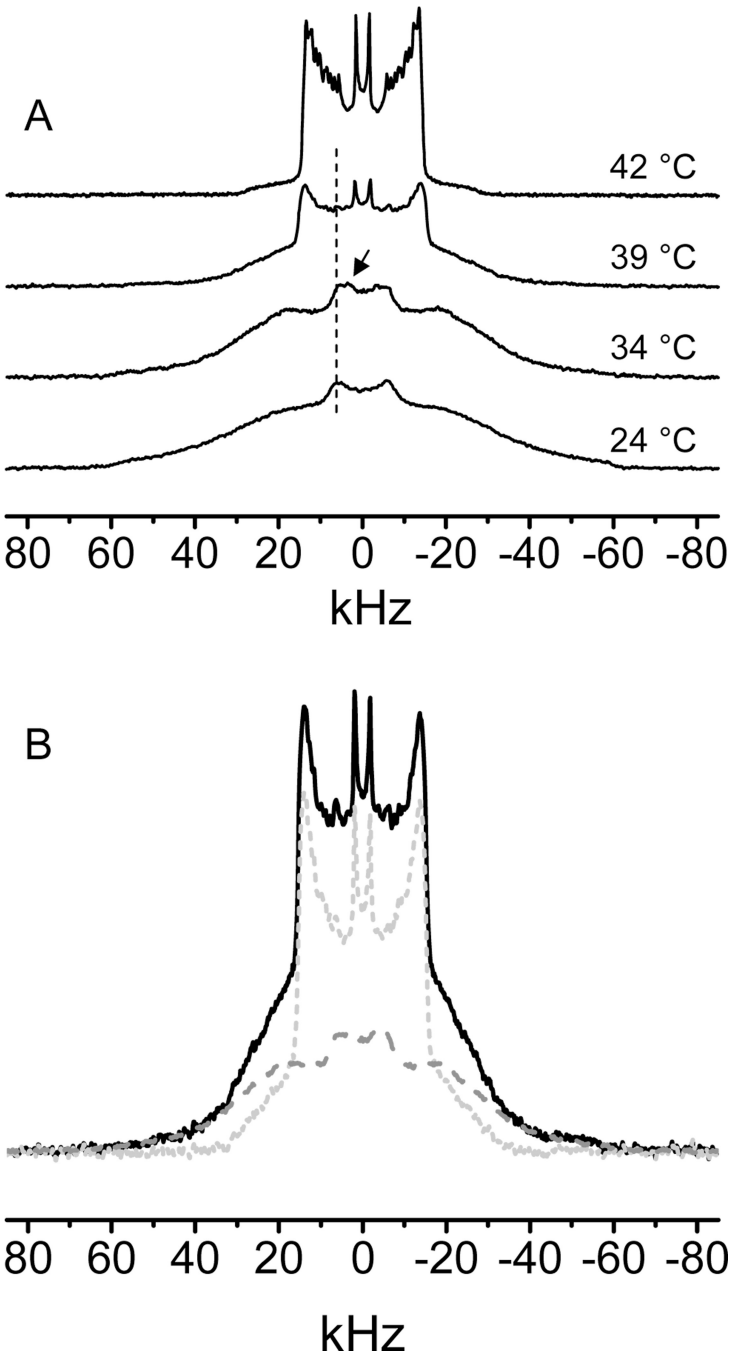

FIGURE 4.

(A) ^{2}H-NMR spectra of DPPC-d_{62} in DPPC collected at 24 °C, 34 °C, 39 °C, and 42 °C. Dotted line serves as a guide to the eye for the L_{β} component of the spectra. Black arrow at 34 °C shows the additional peak in the terminal methyl region of the spectrum indicating a splitting attributed to the onset of the P_{β} phase. (B) Spectral subtraction of the P_{β} spectrum at 34 °C (dashed light grey) from the two component spectrum seen at 39 °C (solid black) yields a spectrum characteristic of DPPC-d_{62} in the L_{α} phase (dashed dark grey).

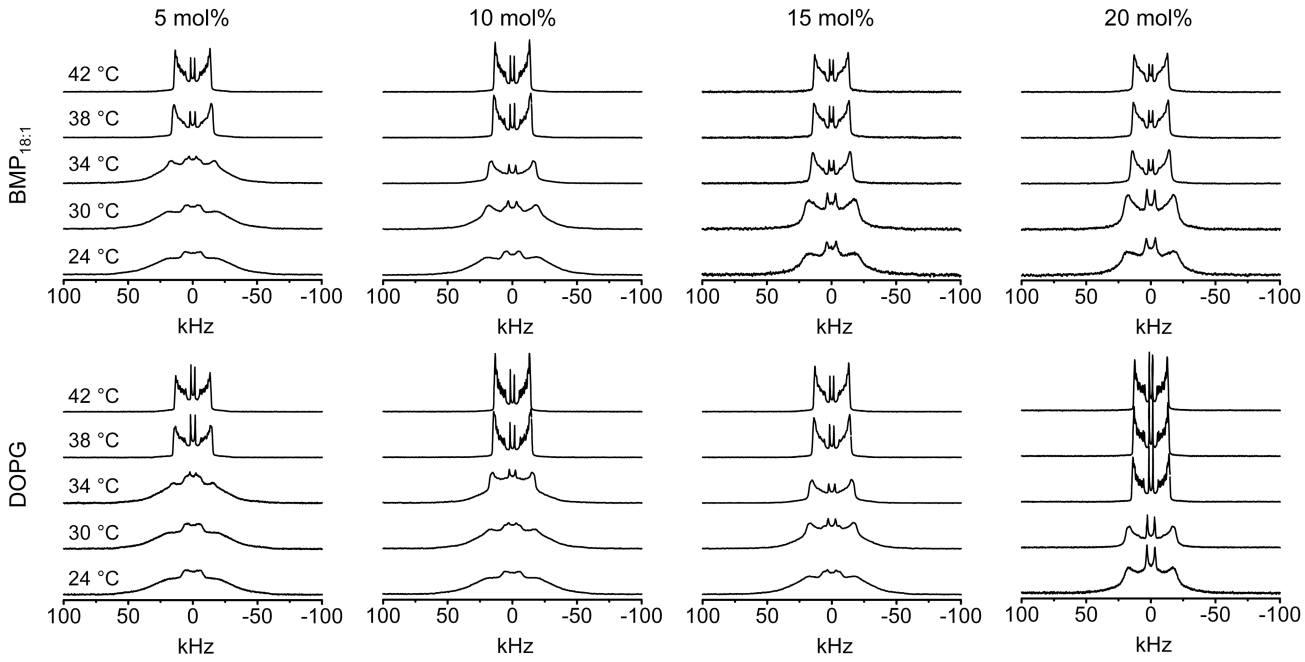

FIGURE 5.

Select ^{2}H-NMR spectra of DPPC-d_{62} in DPPC/$BMP_{18:1}$ mixtures (top) and DPPC/DOPG mixtures (bottom). Spectra shown correspond to those collected at 24 °C, 30 °C, 34 °C, 38 °C, and 40 °C. The mol% of $BMP_{18:1}$ or DOPG increases left to right from 5 to 20 mol% as indicated in the column heading.

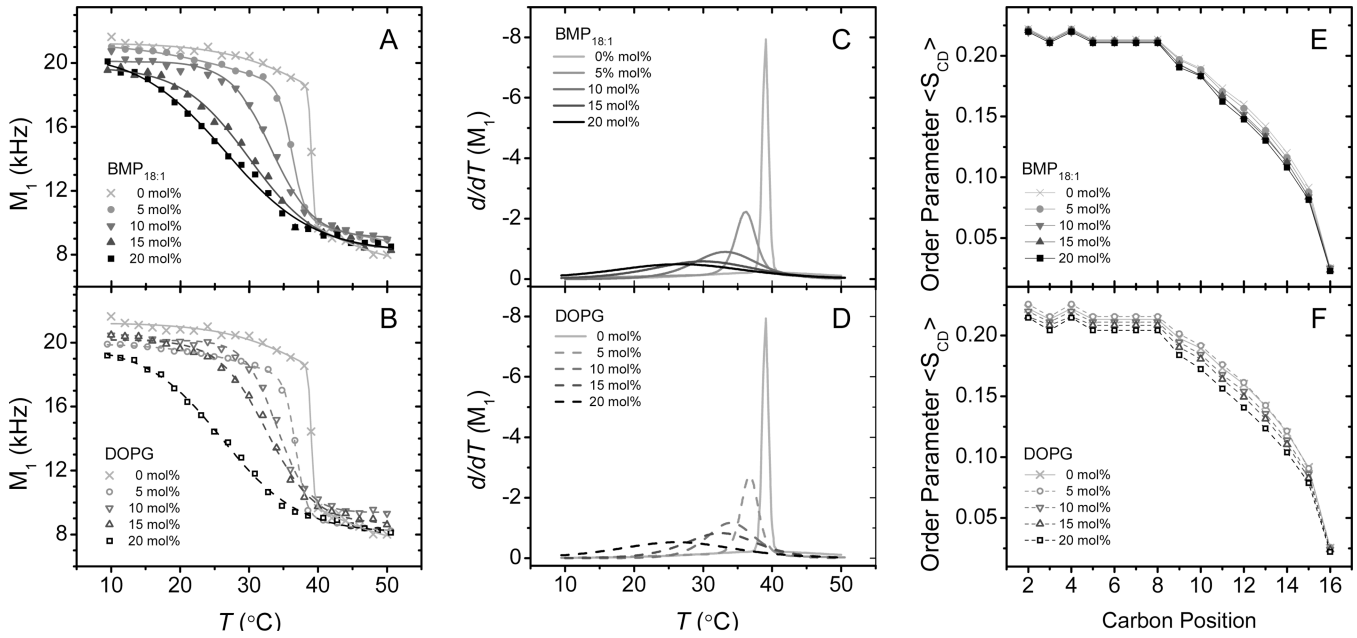

FIGURE 6.

First moment, M_1 analysis of ^{2}H-NMR line shapes as a function of temperature for DPPC-d_{62} in mixtures of (A) DPPC/$BMP_{18:1}$ and (B) DPPC/DOPG. The first moment, M_1, of the ^{2}H NMR spectrum is defined as $\sum|x_n|I_n$, where n corresponds to each data point and I corresponds to the normalized intensity at each frequency x. The lines though the data in (A) and (B) represent fits with either a single or double Boltzmann sigmoid function. Thermal melting curves were obtained as the derivative of the fitted equations with respect to T and are shown for (C) DPPC/$BMP_{18:1}$ and (D) DPPC/DOPG mixtures. Order parameters, $<S_{CD}>$ at 44 °C are plotted as a function of position on the acyl chain for mixtures of (E) DPPC/$BMP_{18:1}$ and (F) DPPC/DOPG.

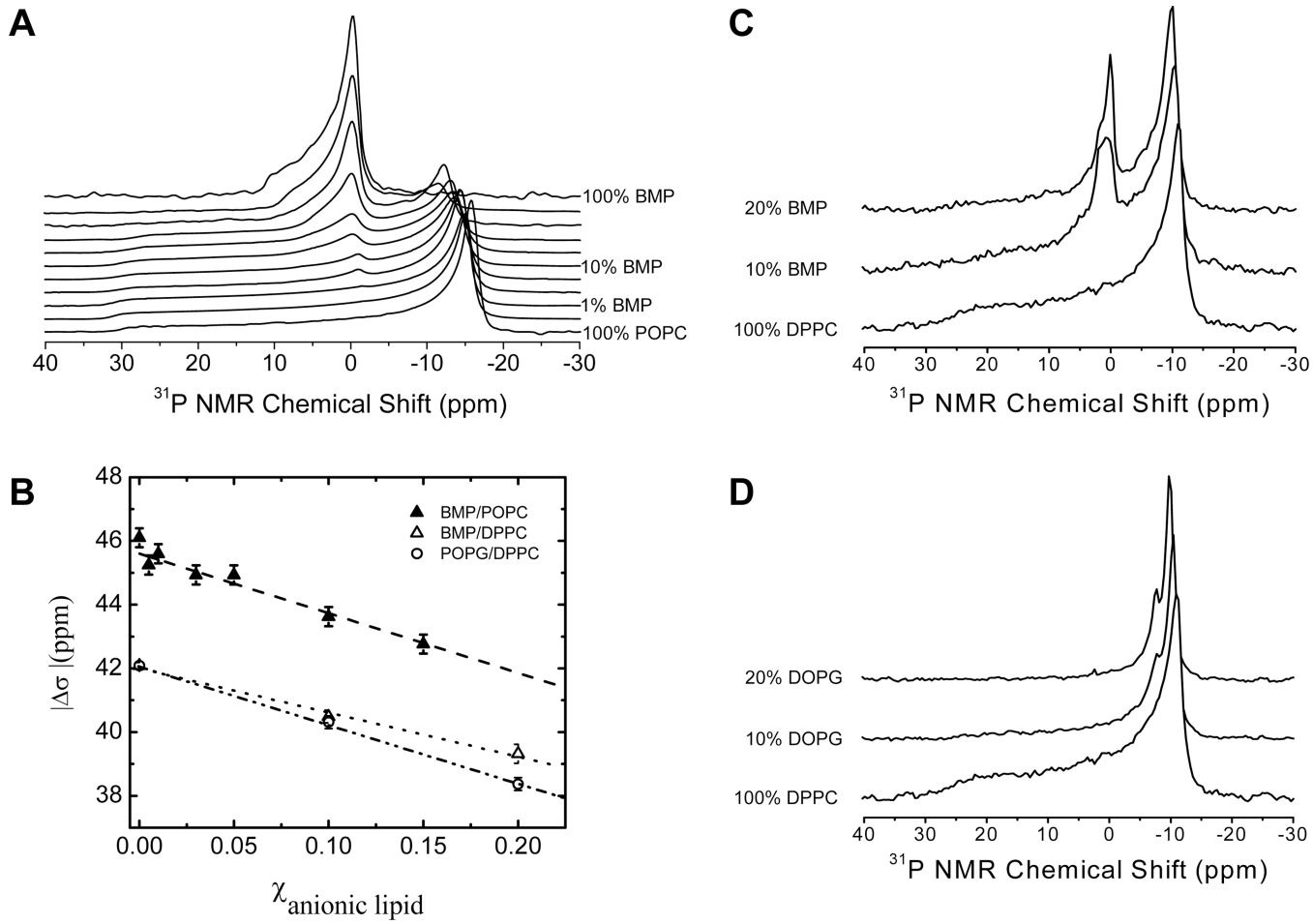

FIGURE 7.

^{31}P NMR investigations of $BMP_{18:1}$ mixing with POPC and DPPC. (A) Stack plot of ^{31}P wide line spectra for varying mol % of BMP collected at 27 °C. From top to bottom: 100, 80, 49, 30, 19, 10, 5, 3, 1, 0.5, 0 mol% BMP. Bottom spectrum is 100% POPC. Samples were prepared in 5 mM Hepes, 100 mM NaCl, 0.1 mM EDTA pH 7.4 (B) Plot of the span ($\Delta\sigma$) of the ^{31}P NMR pattern as a function of mole fraction of anionic lipid (either BMP or DOPG). Stack plots of ^{31}P wide line spectra for (C) $BMP_{18:1}$ and (D) DOPG mixed with DPPC collected at 47 °C prepared in 50 mM NaOAc, 100 mM NaCl, 0.1 mM EDTA pH 4.2. All spectra are referenced to 0 ppm set as the isotropic chemical shift of POPC.

Table 1

Effects of $BMP_{18:1}$ and DOPG on DPPC phase transitions.

	BMP				DOPG			
mol%	T_m (°C)		$\Delta T_{1/2}$ (°C)		T_m (°C)		$\Delta T_{1/2}$ (°C)	
	NMR	***EPR***	***NMR***	***EPR***	***NMR***	***EPR***	***NMR***	***EPR***
0	39.0 ± 0.1	39.5 ± 0.1	0.8 ± 0.8	0.8 ± 0.3	39.0 ± 0.1	39.5 ± 0.1	0.8 ± 0.8	0.8 ± 0.3
5	36.2 ± 0.4	36.1 ± 0.2	3.4 ± 0.6	2.8 ± 0.6	36.7 ± 0.1	36.9 ± 0.4	2.8 ± 0.6	4 ± 2
10	33.2 ± 0.4	N.D.[a]	11.0 ± 1.0	N.D.	34.0 ± 0.3	N.D.	8.0 ± 1.0	N.D.
15	30.0 ± 0.8	28.0 ± 1.0	17 ± 3	19 ± 4	32.6 ± 0.5	29.0 ± 1.0	12 ± 2	19 ± 2
20	26.6 ± 0.9	N.D.	22 ± 3	N.D.	26.1± 0.5	N.D.	20 ± 2	N.D.

[a] In samples for which no EPR data was collected, N.D. (no data) is listed. 95% confidence intervals were propagated from the standard deviations of the x_0, dx, x_2 and k_2 parameters obtained in the Boltzmann and DoubleBoltzmann fits of the first moment (NMR) and second moment (EPR) data.